Biomaterials Science

ROYAL SOCIETY OF CHEMISTRY

PAPER

View Article Online
View Journal | View Issue

Cite this: *Biomater. Sci.*, 2020, **8**, 6637

Matrix stiffness and cluster size collectively regulate dormancy *versus* proliferation in brain metastatic breast cancer cell clusters†

Raghu Vamsi Kondapaneni and Shreyas S. Rao *

Breast cancer cells can metastasize either as single cells or as clusters to distant organs from the primary tumor site. Cell clusters have been shown to possess higher metastatic potential compared to single cells. The organ microenvironment is critical in regulating the ultimate phenotype, specifically, the dormant *versus* proliferative phenotypes, of these clusters. In the context of breast cancer brain metastasis (BCBM), tumor cell cluster–organ microenvironment interactions are not well understood, in part, due to the lack of suitable biomimetic *in vitro* models. To address this need, herein, we report a biomaterial-based model, utilizing hyaluronic acid (HA) hydrogels with varying stiffnesses to mimic the brain microenvironment. Cell spheroids were used to mimic cell clusters. Using 100–10 000 MDA-MB-231Br BCBM cells, six different sizes of cell spheroids were prepared to study the impact of cluster size on dormancy. On soft HA hydrogels (~0.4 kPa), irrespective of spheroid size, all cell spheroids attained a dormant phenotype, whereas on stiff HA hydrogels (~4.5 kPa), size dependent switch between the dormant and proliferative phenotypes was noted (*i.e.*, proliferative phenotype ≥5000 cell clusters < dormant phenotype), as tested *via* EdU and Ki67 staining. Furthermore, we demonstrated that the matrix stiffness driven dormancy was reversible. Such biomaterial systems provide useful tools to probe cell cluster–matrix interactions in BCBM.

Received 12th June 2020,
Accepted 28th September 2020

DOI: 10.1039/d0bm00969e

rsc.li/biomaterials-science

1. Introduction

The ability of breast cancer cells to metastasize to distant organs accounts for ~90% of breast cancer related mortalities.[1,2] Specifically, breast cancer cells are known to metastasize to the lungs, brain, liver, bone, and lymph nodes.[3] In some cases, metastasis may occur even before the detection of the primary tumor.[4] Furthermore, recent studies have demonstrated that collective cell migration (*i.e.*, as a cluster of cells) and dissemination exhibit a significantly higher probability of evolving into metastasis, compared to single cell migration and invasion.[5–7] However, the mechanisms regulating the colonization of organ sites by metastatic tumor cell clusters are not well understood.

Accumulating evidence suggests that there is a latency period between dissemination and metastatic outgrowth.[8,9] During this period, tumor cells may attain a dormant state, where the cells are either growth-arrested (cellular dormancy) or the cell growth is balanced by apoptosis occurring within the tumor (mass dormancy).[9] Disseminated tumor cells are capable of developing metastasis, even after sustaining an extended period of dormancy for decades.[8–10] Despite the progress in developing therapeutic strategies, the 5-year survival rate for patients with breast cancer metastasis in the United States is only 26%.[11] Breast cancer brain metastasis (BCBM) is the most aggressive with a median survival period of only 4–16[12] months. This is mostly attributed to poor prognosis and, in part, to the lack of understanding of the underlying mechanisms involved in tumor relapse at the metastatic site. This is further hampered by the lack of relevant experimental model systems to study and elucidate the underlying mechanisms involved in the reawakening of dormant BCBM cells.

It is now well recognized that the tumor microenvironment plays a significant role in modulating the dormant phenotype of disseminated tumor cells,[8,9,13–15] consistent with the "seed and soil" theory proposed in 1889.[16] Specifically, the extracellular matrix (ECM) is critical in determining the fate of disseminated tumor cells.[17,18] In order to develop an *in vitro* model to study tumor dormancy, it is imperative to incorporate the ECM to capture the cell–ECM interactions. To this end, many studies have utilized various natural, synthetic, and semi-synthetic biomaterials to mimic the ECM, such as base-

Department of Chemical and Biological Engineering, The University of Alabama, Tuscaloosa, Alabama 35487, USA. E-mail: srao3@eng.ua.edu; Fax: +1 (205) 348-7558; Tel: +1 (205) 348-6564

†Electronic supplementary information (ESI) available. See DOI: 10.1039/d0bm00969e

ment membrane matrix (Matrigel),[19–21] collagen,[22,23] fibrin gel,[24] hyaluronic acid (HA),[25] polyethylene glycol (PEG),[26] polyacrylamide[27] and Amikagel[28] to study the regulation of dormancy in the context of the primary tumor setting.

Few studies have been reported to investigate tumor dormancy in the metastatic setting. For example, dormancy in bone metastatic breast cancer cells has been studied by using biomaterial-based[29] and bioreactor-based models,[30] whereas microfluidic-based co-culture models have been used to study dormancy in liver metastatic breast cancer cells.[31,32] More recently, our group reported a HA hydrogel based platform to investigate dormancy in BCBM cells at the single cell level.[12] These models provide insightful information about the mechanisms regulating tumor dormancy at a single cell level. However, to the best of our knowledge, there are no reported *in vitro* models investigating dormancy in BCBM cell clusters.

Herein, we report an *in vitro* biomaterial-based model to study microenvironmental regulation of dormancy in BCBM cell clusters. We utilized HA hydrogels to mimic the native brain ECM, as HA is one of the most abundant components of the brain ECM and is highly secreted in brain metastatic lesions.[33,34] We prepared two versions of the HA hydrogels, namely soft (*i.e.*, 0.4 kPa) and stiff (*i.e.*, 4.5 kPa) HA hydrogels, which bracketed the native brain stiffness and that reported for brain metastasis.[12] Tumor cell spheroids were employed to mimic cell clusters. To study the effect of cluster size, six different sizes of cell spheroids were prepared by using 100–10 000 BCBM cells. Cell spheroids were cultured on top of both the hydrogels to evaluate the effect of matrix stiffness on dormancy *vs.* proliferation of cell clusters. Cell spheroids were also cultured in suspension and adherently (*i.e.*, on tissue culture polystyrene (TCPS)) to investigate the effect of culture conditions on cell cluster phenotypes. Finally, we also tested the reversibility of the dormant phenotype in this system.

2. Experimental

2.1. Cell culture

td-Tomato expressing MDA-MB-231Br, a brain metastatic breast cancer cell line, derived from a triple negative breast cancer cell line MDA-MB-231 was used in this study and was cultured as described previously.[12] Briefly, the cells were maintained in Dulbecco's Modified Eagle's Medium (DMEM) high glucose (Sigma Aldrich) media supplemented with 10% fetal bovine serum (FBS) (VWR Life Science) and 1% penicillin–streptomycin (PS) (Gibco) at 37 °C and in a 5% CO_2 environment.

2.2. HA hydrogel preparation

Synthesis of hyaluronic acid methacrylate (HAMA) was performed using previously established procedures.[12,35,36] Briefly, a 1 wt% solution of sodium hyaluronate (66–90 kDa; Lifecore Biomedical) was prepared in deionized water overnight and subjected to ~18 fold molar excess of methacrylic anhydride (Sigma Aldrich) at 4 °C, by maintaining the pH between 8 and 10 using 5 M NaOH. A five-fold volumetric excess of cold acetone was added to the reaction mixture to extract HAMA, which was then flash frozen and lyophilized overnight. Proton nuclear magnetic resonance (^{1}H NMR) was utilized to measure the degree of methacrylation and in this study HAMA with ~85% degree of methacrylation was used. Next, a gel precursor solution was prepared using 5 wt% HAMA solution in DMEM and dithiothreitol (DTT) (Sigma Aldrich), and 80 μL of this solution was added to each well of a 96-well plate and incubated overnight for gelation. Different concentrations of DTT were used to obtain hydrogels with varying stiffnesses *i.e.*, 10 mM for the soft hydrogel (~0.4 kPa) and 40 mM for the stiff hydrogel (~4.5 kPa), respectively, as determined *via* compression testing using a RSA-G2 solid analyzer (TA Instruments).[12,36] To enhance cell adhesion, surfaces of both soft and stiff HA hydrogels were consistently functionalized with an integrin binding peptide (RGD) (Anaspec) as reported previously.[36]

2.3. Tumor cell spheroid construction

Cell spheroids were prepared utilizing a previously established protocol.[37] Briefly, 20 mg ml^{-1} poly(2-hydroxyethyl methacrylate) (p-HEMA) (Sigma Aldrich) solution was prepared by dissolving 500 mg of p-HEMA in 25 mL of 95% ethanol for 3 h. Each well of a 96 well conical bottom plate (Thermo Fisher Scientific) was coated with ~30 μL of p-HEMA solution to create an ultralow attachment surface for cells, followed by drying the plate overnight in a laminar hood. Next, cell dilutions were prepared based on the cell count needed to prepare spheroids. 100 μL of cell suspension containing the required cell count of MDA-MB-231Br cells was added to the wells of a p-HEMA coated 96-well conical bottom plate and the plate was centrifuged at ~1000*g* for 10 min. After centrifugation, 2.5% of growth factor reduced Matrigel (Corning) was added to the wells on v/v basis and the plate was incubated overnight. On the following day, cell spheroids were collected using a 200 μL pipette with the tip removed to minimize spheroid disintegration and subsequently cultured on top of the soft or stiff HA hydrogel or as a suspension culture on p-HEMA coated flat 96-well plate or as adherent culture on TCPS.

2.4. Optical imaging and cell spheroid area measurements

Cell spheroids cultured under different culture conditions were monitored daily using an Olympus IX83 microscope with a spinning confocal disc attachment. Both bright field and fluorescent images of cell spheroids were captured throughout the culture period to track their growth. Specifically, day 0 images were taken within half an hour post transfer of cell spheroids. Image-J software was used to measure the cell spheroid area (cross sectional area of spheroid + spread area of cells (in case cells were migrating from spheroids)) as described earlier.[38,39] Briefly, the boundary of the cell spheroids was manually selected and if migration was observed from spheroids, their boundaries were also considered to calculate the spheroid areas.

2.5. Dissociation of cell spheroids

For quantification at the single cell level, cell spheroids were dissociated into single cells before staining for various markers. Dissociation of cell spheroids into single cells was performed by adopting the procedure described previously.[40] Briefly, cell spheroids were collected on day 7 in an Eppendorf tube and the media was removed, and the spheroids were washed twice with 300 μL of 1× phosphate buffered saline (PBS) (Gibco). Next, 300 μL of Accutase (Corning) was added to the spheroids and incubated for ~5 min at 37 °C. After 5 min of incubation, the spheroids were resuspended in Accutase using a 200 μL pipette tip to mechanically disintegrate the spheroids for another ~5 min followed by an additional incubation of ~5 min. This cycle was repeated for ~40 min and the Eppendorf tubes were centrifuged for allowing the cells to settle to the bottom. The single cells were then washed twice with PBS and transferred to a 96 well plate for staining.

2.6. 5-Ethynyl-2′-deoxyuridine (EdU) cell proliferation assay

The proliferation of cell spheroids under various culture conditions for a period of 7 days was measured by incorporating EdU (Click-iT® EdU Microplate Assay Kit (Invitrogen C10214)) into the cell DNA as described in previous studies.[12,38] Briefly, on day 7, media in each well were replaced with 10 μM EdU containing media and incubated overnight. The media were then removed and the spheroids were dissociated into single cells and transferred into a 96 well plate and fixed for ~5 min by adding 50 μL of the click-iT® EdU fixative. Next, 50 μL of the reaction cocktail prepared as per manufacturer's protocol was added to the wells and incubated for 25 min in the dark at room temperature. After incubation, the plate was centrifuged at 1000*g* for 1 min, followed by washing twice with PBS. The cells were then counterstained with DAPI (Invitrogen) for 5 min in the dark at room temperature. An Olympus IX83 microscope with a spinning confocal disc attachment was used for fluorescence microscopy. Exposure time and gain settings were maintained constant for all the conditions. Multi point tool in ImageJ software was utilized to quantify %EdU positive cells, as described previously.[12]

2.7. Immunofluorescence staining

On day 7, the cell spheroids cultured under various culture conditions were collected and dissociated into single cells and transferred into a 96 well plate and washed twice with 100 μL of PBS. Next, the cells were fixed at room temperature for 20 min by adding 100 μL of 4% paraformaldehyde, permeabilized in the presence of 0.25% TritonX-100 in 1× PBS for 15 min at room temperature and blocked by adding 5% bovine serum albumin (BSA) in 1× PBS for 30 minutes at 4 °C. Between each step, the cells were washed with PBS and before aspirating any solution, the plate was centrifuged at 1000*g* for 1 min. The cells were then stained for Ki67 protein (ab15580, Abcam) (marker for cell proliferation), cleaved caspase-3 (Asp175, Cell Signaling Technology), vimentin (SC-6260, Santa Cruz Biotechnology), or E-cadherin (SC-21791, Santa Cruz Biotechnology).

The cells were incubated overnight at 4 °C with 100 μL of primary antibody dilutions (1 : 150 for Ki-67, 1 : 200 for vimentin, E-cadherin, and cleaved caspase-3, respectively,) in 1× PBS. On the following day, the cells were washed twice with 1× PBS and incubated at 4 °C for 1 hr with 100 μL of fluorescently labeled secondary antibody dilutions (1 : 1000) in 1× PBS. Alexa Fluor 488-conjugated goat anti-rabbit secondary antibody (A11034, Invitrogen) was used to detect Ki-67 and cleaved caspase-3. Alexa Fluor 488-conjugated goat anti-mouse secondary antibody (A11001, Invitrogen) was utilized to detect vimentin and E-cadherin. Later, the cells were counterstained with DAPI for 5 min at room temperature. An Olympus IX83 microscope with a spinning confocal disc attachment was used for fluorescence microscopy. Exposure time and gain settings were maintained constant for all conditions. Multi point tool in ImageJ software was utilized to quantify % Ki67 positive, % vimentin positive, and % cleaved caspase-3 positive cells, as described previously.[12] A similar protocol was followed for staining cell spheroids. Cell spheroids were also directly stained for F-actin using AlexaFluor-488 labeled phalloidin (A12379, Invitrogen) using a dilution of 1 : 500.

2.8. Apoptosis assay

In addition to cleaved caspase-3 staining, Annexin-V Apoptosis Detection Kit (Santa Cruz Biotechnology) was used to detect the % apoptotic cells present in 10k cell spheroids by following the protocol prescribed by the manufacturer. Briefly, on day 7, cell spheroids were dissociated into single cells. Single cells were washed twice with PBS and once with 1× assay buffer solution. After washing, 100 μL of 1× assay buffer solution and ~2.5 μL of FITC-conjugated Annexin-V was added to the cells and incubated for 15 min in the dark at room temperature. The cells were then washed twice with PBS. Before aspirating any solution from the wells, the plate was centrifuged at 1000*g* for 1 min to allow the cells to settle to the bottom. An Olympus IX83 microscope with a spinning confocal disc attachment was used for fluorescence microscopy. Exposure time and gain settings were maintained constant for all the conditions. Multi point tool in ImageJ software was utilized to quantify % apoptotic cells, as previously described.[12]

2.9. Statistical analysis

All the experiments were performed at least twice with at least 2 replicates for each condition. The data are reported as mean ± standard error unless otherwise mentioned. Statistical analysis was performed using JMP Pro software. Student's *t*-test or ANOVA followed by Tukey's HSD *post-hoc* analysis was performed to compare samples depending on the number of available data sets. A statistically significant difference between the data sets was noted for *p*-value less than 0.05.

3. Results and discussion

In this study, we report an *in vitro* biomaterial based-model, to investigate the impact of ECM stiffness and cell cluster size on the dormant *vs.* proliferative status of brain metastatic breast cancer cell clusters by utilizing various sizes of MDA-MB-231Br cell spheroids and HA hydrogels with varying stiffnesses. The impact of ECM stiffness on the behavior of tumor cells at the single cell level has been extensively studied in the context of a primary tumor setting,[11,19,20,23–27,41] however, relatively few studies have been reported in the metastatic setting.[12,29,36] Herein, for the first time, we studied the influence of ECM stiffness on BCBM cell clusters, as they are known to possess higher metastatic potential. Furthermore, cell–matrix interactions involved in establishing BCBM are not well understood. To this end, we elucidated the effect of various culture conditions on BCBM cell spheroids by culturing them as suspension and adherent cultures in addition to culture on ECM mimicking HA hydrogels.

3.1. Effect of culture conditions and cell spheroid size on the phenotype of BCBM cell spheroids

Despite the fact that tumor cell clusters possess higher metastatic potential compared to single cells, the interaction between tumor cell clusters and the brain microenvironment is not well understood. Here, soft (0.4 kPa) and stiff (4.5 kPa) HA hydrogels were formulated to simulate the stiffness range of the native brain ECM (0.2–1 kPa (ref. 42)) and that noted for metastatic brain malignancy (3.7 kPa (ref. 43)). HA hydrogels were formed by altering the crosslinker concentrations while maintaining a similar HA composition. To assess the impact of culture conditions, we cultured brain metastatic breast cancer cell spheroids in suspension culture, adherent culture on 2D TCPS, and on top of the brain ECM mimicking soft (0.4 kPa) and stiff HA (4.5 kPa) hydrogels. To date, circulating tumor cell (CTC) clusters composed mostly of 2 to 100 cells have been detected clinically.[44] Here, to assess the impact of cluster size, cell spheroids were prepared by using six different cell densities (*i.e.*, 100, 500, 1k, 2k, 5k and 10k cells), including the clinically observed 100 cell clusters.[44] Optical imaging showed that uniform and reproducible cell spheroids were formed within 24 h. These cell spheroids were then transferred to different culture conditions on the next day and cultured for 7 days. Day 0 bright field and fluorescent images of cell spheroids (Fig. 1a and b) show that the cells were compactly positioned in the spheroids and no scattering of cells was seen even after the transfer of the spheroids. To assess the growth profile of cell spheroids, the area of the cell spheroids was measured each day throughout the culture period.

Cell spheroids cultured adherently on 2D TCPS exhibited an enhanced growth profile, where the cells started to spread on TCPS and in the case of higher cell density spheroids more than half of the well plate area was covered with cells by the end of day 7 (Fig. S1–S6†). As a result, the day 7 area of all the cell spheroids was at least 10 times greater than the day 0 areas. Thus, only the area of cell spheroids cultured in suspension, and on soft or stiff HA hydrogel was plotted to show the impact of culture conditions on cell spheroids (Fig. 1c–h). In the case of 100 and 500 cell spheroids, spheroids cultured in suspension displayed a linearly increasing growth trend as the cell spheroid areas increased from day 0 to day 7 (Fig. S1 and S2†). Specifically, for the 100 cell spheroid, the day 7 area in the suspension culture ($37\,699 \pm 8624\ \mu m^2$) was ~4 times higher compared to the day 0 area ($8828 \pm 321\ \mu m^2$) and for the 500 cell spheroid, the day 7 area in the suspension culture was ~7 times greater compared to the day 0 area. In contrast, the areas of 100 and 500 cell spheroids cultured on the soft or stiff HA hydrogel remained mostly constant throughout the culture period (Fig. 1c and d). For 1k and 2k cell spheroids, day 7 spheroid areas for suspension culture were ~7 times higher than the day 0 area and the areas of 1k and 2k cell spheroids cultured on the soft HA hydrogel remained largely unchanged from day 0 to day 7. However, a slight increase in the area was noted by the end of day 7 for 1k and 2k cell spheroids cultured on the stiff HA hydrogel compared to the soft HA hydrogel, although this change was not statistically significant (Fig. 1e and f).

Even though similar growth profiles were observed for 5k and 10k cell spheroids when cultured in suspension, the fold increase in the area over 7 days for 5k (~5 times) and 10k (~2.75 times) cell spheroids was less when compared to 500, 1k and 2k (>7 times) cell spheroids. When cultured on the soft HA hydrogel, both 5k and 10k cell spheroids exhibited a dormant phenotype, wherein the cell spheroid area was mostly unchanged throughout the culture period. In contrast, on the stiff HA hydrogel, areas of both 5k and 10k cell spheroids increased significantly ($p < 0.05$), as the day 7 area of both the cell spheroids was ~1.8 fold higher compared to those on the soft HA hydrogel (Fig. 1g and h). Based on area measurements, BCBM cell spheroids exhibited three different phenotypic growth patterns depending on the culture environments. When BCBM cell spheroids were cultured either in suspension or adherent cultures, they exhibited a proliferative phenotype as expected (Fig. 1, and S1–S6†). When BCBM cell spheroids were cultured on top of soft HA hydrogels, they exhibited a dormant phenotype compared to stiff HA hydrogels (Fig. 1). Furthermore, cell spheroids cultured on top of stiff HA hydrogels displayed a size dependent switch between dormant and proliferative phenotypes (Fig. 1).

Interestingly, stiffness mediated cell migration from cell spheroids and micro-colony formation were observed for 10k cell spheroids cultured on the stiff HA hydrogel by day 7. In contrast, when the 10k cell spheroids were cultured on the soft HA hydrogel for a period of 7 days, the spheroids displayed the same morphology throughout the culture time (Fig. 2a and b). This is consistent with observations made by Ondeck *et al.*, who also recently showed that on stiff methacrylated HA substrates (~5 kPa), cells tend to migrate away from mammary epithelial cell spheroids.[45] In 10k cell spheroids cultured on the stiff HA hydrogel, no cell migration was observed by the end of day 1 (Fig. 2c), however, by the end of day 7, we noticed cell migration and micro-colony formation at a significant distance

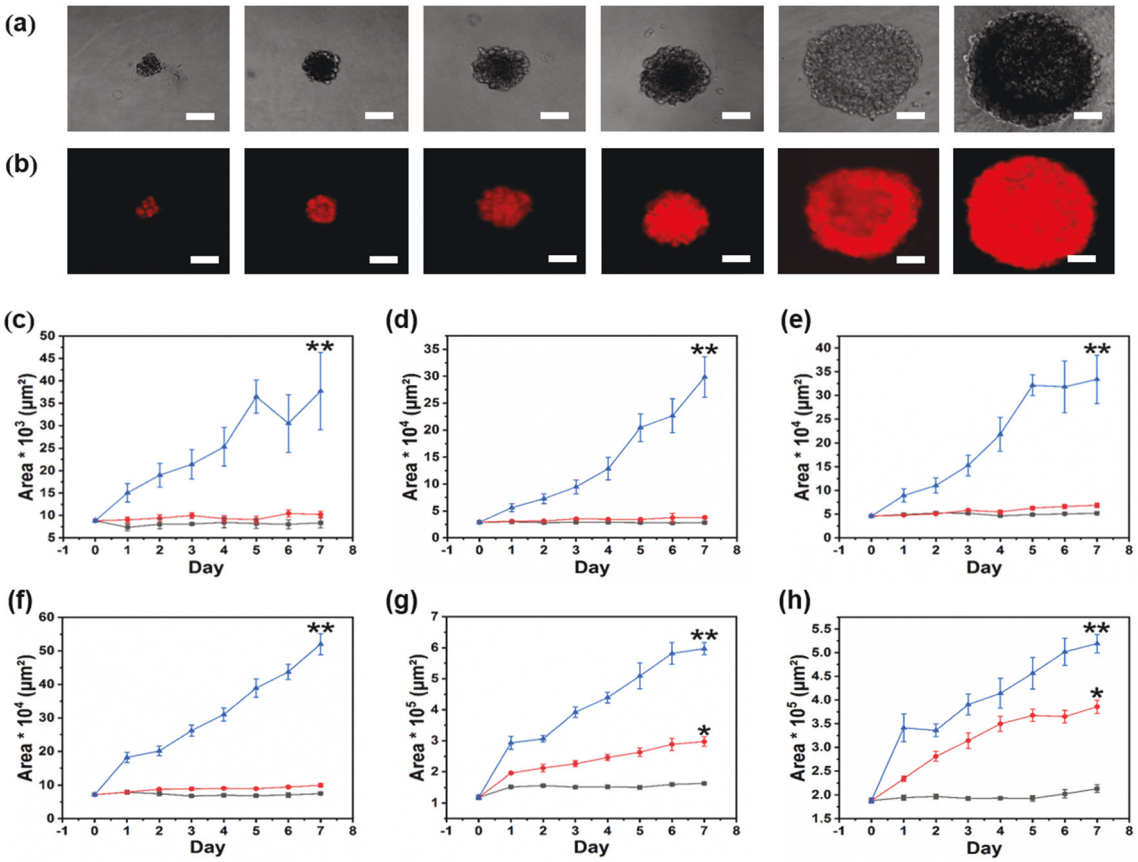

Fig. 1 Brain metastatic breast cancer cell spheroids exhibited differential growth responses over a period of 7 days depending on the culture conditions and spheroid size. (a) Bright field and (b) florescent images (day 0) of cell spheroids prepared using 100, 500, 1k, 2k, 5k and 10k MDA-MB-231Br cells (from left to right). Scale bar = 100 μm. Area of cell spheroids under various culture conditions for (c) 100 cell spheroids, (d) 500 cell spheroids, (e) 1k cell spheroids, (f) 2k cell spheroids, (g) 5k cell spheroids and (h) 10k cell spheroids over a period of 7 days. Blue – suspension culture, red – stiff HA hydrogel (4.5 kPa), and black – soft HA hydrogel (0.4 kPa). $N \geq 5$ replicates per condition. **Indicates statistical significance ($p < 0.05$) compared to both soft and stiff HA hydrogel conditions for the area at day 7. *Indicates statistical significance ($p < 0.05$) compared to the soft HA hydrogel for the area at day 7. Error bar represents standard error.

(375 ± 61 μm) from the spheroids (Fig. 2d i, ii and e). Interestingly, uniform cell migration was not observed throughout the periphery of the spheroid (Fig. 2d iii and iv) as seen on 2D TCPS (Fig. S6†). The maximum area of the micro-colonies formed was similar to that of the 100 cell spheroid area; these micro-colonies were as compact as those of the 100 cell spheroid (Fig. 2d v). Taken together, these results indicate that the culture environment, size of the cell clusters, and the ECM stiffness play a crucial role in modulating the growth phenotype of cell clusters.

3.2. ECM stiffness driven dormancy and proliferation in BCBM cell spheroids

As the cell spheroids cultured on top of the soft or stiff HA hydrogel displayed a dormant *vs.* proliferative phenotype, we sought to quantify the percentage of proliferating cells present in the cell spheroids. First, we utilized Ki67 staining to detect the Ki67 protein, which is used as a marker for cell proliferation, as it is highly expressed during the active phases of the cell cycle and is absent when the cells are either in a dormant or quiescent phase.[46,47] Also, many studies have utilized Ki67 as a marker to study dormancy.[12,22,29,31] We initially stained the cell spheroids cultured on both soft and stiff HA hydrogels directly on day 7 for Ki67. We found that 100, 500, 1k and 2k cell spheroids were largely Ki67 negative (Fig. S7–S10†) regardless of hydrogel stiffness. However, the 5k and 10k cell spheroids cultured on the stiff HA hydrogel showed some Ki67 positivity indicating the presence of proliferating cells compared to the spheroids cultured on the soft HA hydrogel (Fig. S11 and S12†). Ki67 staining of cell spheroids directly, qualitatively demonstrated size-dependent dormant *vs.* proliferative phenotypes on the stiff HA hydrogel and a dormant phenotype on the soft HA hydrogel irrespective of the cluster size. Interestingly, micro-colonies of 10k cell spheroids formed on the stiff HA hydrogel exhibited Ki67 positivity (Fig. S13†), however, those of similar sized 100 cell spheroid were largely Ki67 negative when seeded directly on the stiff HA hydrogel (Fig. S7†).

To obtain quantitative results, we dissociated the spheroids into single cells and stained them for Ki67. For this analysis,

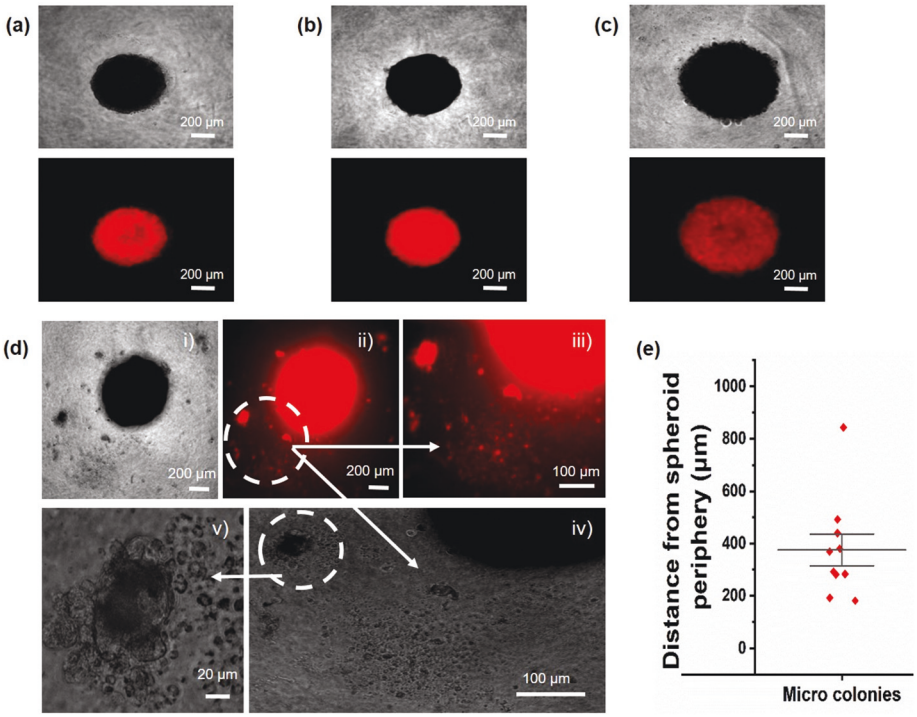

Fig. 2 Stiffness and size-induced migration and formation of micro-colonies were observed in 10k cell spheroids when cultured on a stiff HA hydrogel (4.5 kPa) as opposed to those cultured on a soft HA hydrogel (0.4 kPa). (a) Day 1 and (b) day 7 bright field and florescent images of 10k cell spheroids cultured on a soft HA hydrogel. (c) Day 1 and (d) day 7 bright field and florescent images of 10k cell spheroids cultured on a stiff HA hydrogel and (e) distance of micro-colonies from the spheroid periphery. $N \geq 8$ replicates per condition.

we used only the 10k cell spheroid, given the dramatic differences in stiffness induced growth characteristics observed under this condition (Fig. 1). On day 7, spheroids cultured on top of HA hydrogels were collected and disintegrated into single cells. Ki67 staining of these single cells revealed that spheroids cultured on the stiff HA hydrogel had a 2 fold higher population of Ki67 positive cells compared to those on the soft HA hydrogel ($p < 0.05$). Specifically, 11.7 ± 1.6% cells were Ki67 positive when cultured on the soft HA hydrogel *vs.* 27.7 ± 2.3% on the stiff HA hydrogel (Fig. 3). Single cells obtained from the 10k cell spheroid cultured in suspension and adherent cultures were also stained for Ki67, indicating 32.6 ± 0.2% Ki67 positive cells present in the suspension culture, and 52.6 ± 3.8% Ki67 positive cells in the adherent culture (Fig. 3). The number of Ki67 positive cells present in the 10k cell spheroids cultured in suspension and adherent cultures was significantly higher when compared to those on the soft HA hydrogel ($p < 0.05$).

In addition to Ki67, we also evaluated the % of proliferating cells present in the 10k cell spheroids by incorporating EdU into the newly synthesized DNA. EdU incorporation has been widely used to measure cell cycle progression (*G*0/*G*1 transition) and as a marker to study cancer dormancy.[11,12,31,38,48] EdU staining was carried out on day 7 for 10k cell spheroids cultured on the soft or stiff HA hydrogel, as well as suspension and adherent cultures. Consistent with Ki67 staining, we found that % of EdU positive cells present in 10k cell spheroids was significantly higher in the stiff HA hydrogel compared to the soft HA hydrogel ($p < 0.05$). In particular, 16.4 ± 1.5% of EdU positive cells were present in the spheroids cultured on the soft HA hydrogel compared to 37.5 ± 0.9% of EdU positive cells in the stiff HA hydrogel (Fig. S14†). The percentage of EdU positive cells was significantly higher ($p < 0.05$) in the 10k cell spheroids cultured in suspension (54.9 ± 2.2%) and adherent cultures (72.8 ± 1.5%) compared to spheroids cultured on both soft and stiff HA hydrogels (Fig. S14†).

To gain mechanistic insights, we performed immunofluorescence staining for vimentin (mesenchymal marker), E-cadherin (epithelial marker) and F-actin for the 10k cell spheroids. We observed an increase in the % of vimentin-positive cells in 10k cell spheroids on the stiff HA hydrogel compared to those on the soft HA hydrogel (*i.e.*, 50.8 ± 3.2% *vs.* 35.8 ± 3.3%) (Fig. S15 and S16†). MDA-MB-231Br cells are derived from MDA-MB-231 (parental cell line), and exhibit mesenchymal characteristics.[49] Thus, as expected, the % of E-cadherin positive cells was low (<2%), and similar on both soft and stiff HA hydrogels (not shown). Migrating cells from 10k cell spheroids on the stiff HA hydrogel exhibited a spread morphology at the spheroid periphery and near the micro-colonies (Fig. S17 and S18†) with a developed actin cytoskeleton, whereas on the soft HA hydrogel no protrusions were seen along the periphery of the 10k cell spheroids (Fig. S19†). Size dependent dormant *vs.* proliferative phenotypes observed on the stiff HA hydrogel can also be partly attributed to a signifi-

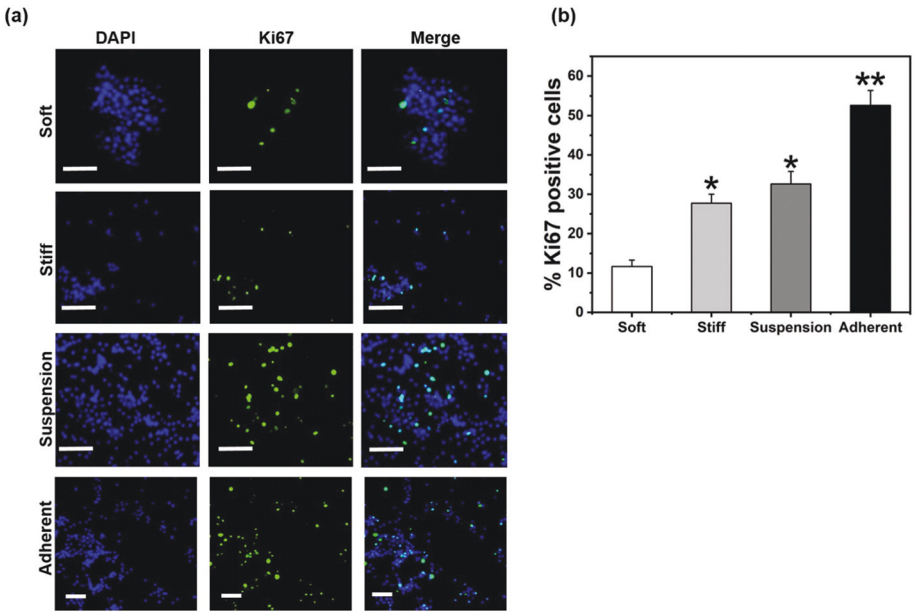

Fig. 3 Brain metastatic breast cancer cells in 10k spheroids cultured on the soft HA hydrogel (0.4 kPa) were Ki67 negative and displayed a dormant phenotype compared to those on the stiff HA hydrogel (4.5 kPa). (a) Representative fluorescent images of Ki67 staining for MDA-MB-231Br cells obtained from 10k spheroids cultured under various culture conditions. Blue – DAPI (nucleus) and green – Ki67. Scale bar = 100 μm. (b) Quantification of Ki67 positive cells in 10k spheroids cultured on soft or stiff HA hydrogel, suspension, and adherent cultures, respectively. $N \geq 4$ replicates per condition. **Indicates statistically significant difference ($p < 0.05$) compared to the soft and stiff HA hydrogel and suspension culture. *Indicates statistically significant difference ($p < 0.05$) compared to the soft HA hydrogel. Error bar indicates standard error.

cant increase ($p < 0.05$) in the percentage of vimentin positive cells in larger clusters (50.8 ± 3.2% positive cells in the 10k cell spheroid) compared to small clusters (40.6 ± 1.9% positive cells in 500 cell spheroids). Furthermore, % EdU positive cells present in the 500 cell spheroid were significantly lower (13.5 ± 1.3%) compared to the 10k cell spheroids (37.5 ± 0.9%) cultured on the stiff HA hydrogels ($p < 0.05$).

Annexin-V and cleaved caspase-3 staining were utilized to quantify apoptotic cells present in the 10k cell spheroids and to examine whether the observed dormant phenotype on the soft HA hydrogel is due to apoptosis. The percentage of apoptotic cells present in 10k cell spheroids cultured on both soft and stiff HA hydrogels was similar and less than 11% (Fig. S20 and S21†). In particular, the spheroids contained 7.4 ± 1% Annexin V positive cells in the soft HA hydrogel compared to 5.1 ± 1.1% in the stiff HA hydrogel. Similarly, 11.2 ± 3.2% cells stained positive for cleaved caspase-3 in the soft HA hydrogel compared to 7.6 ± 0.9% in the stiff HA hydrogel. This result suggests that the dormancy observed on the soft HA hydrogel is primarily due to the ECM stiffness and not due to cell death by apoptosis. In summary, these results demonstrated that spheroids cultured on a soft HA hydrogel exhibited a dormant phenotype in comparison with the spheroids cultured on a stiff HA hydrogel that exhibited a size dependent dormant *vs.* proliferative phenotype. Previously, Singh *et al.*, reported that size dependent migratory characteristics were exhibited by three dimensional breast cancer micro-tumors when cultured on non-adhesive PEG dimethacrylate hydrogel microwells.[50,51] Herein, we were able to establish a cluster size cut off range for the dormant *vs.* proliferative phenotype on the stiff HA hydrogel for the first time depending on the initial number of cells present in the cluster (*i.e.*, proliferative phenotype ≥5000 cells < dormant phenotype). Thus, our data suggest that matrix stiffness and cluster size collectively determine the dormant *vs.* proliferative phenotype. Based on prior studies,[28,50,52] it is possible that necrotic cores may be present in 10k cell spheroids (diameter >400 μm) and may also play a role in the observed phenotype. This would be investigated in future studies.

3.3. Reversibility of the ECM stiffness induced dormant phenotype

Reawakening of dormant tumor cells or cell clusters by microenvironmental derived cues has been known to contribute to disease relapse at the metastatic site.[9,11,13] Modifications to the ECM, which results in the reawakening of single dormant cancer cells, have been previously reported *in vitro*.[11,12,19,23,28,45] For instance, Barkan *et al.*, demonstrated that the incorporation of fibronectin into the ECM (cultrex) drove quiescent single D2.0R breast cancer cells into a proliferative state.[19] A recent study by Pradhan *et al.*, showed that dormant MDA-MB-231 breast cancer cells can be activated by increasing the adhesiveness of the matrix.[11] In the context of reversing ECM stiffness driven dormancy, Grandhi *et al.*, showed that when dormant 100k T24 (bladder cancer) cell spheroids cultured on ~216 kPa Amikagels were transferred to ~36 kPa Amikagels, cell shedding and micro-colony formation were observed.[28] Herein, we tested whether the ECM stiffness

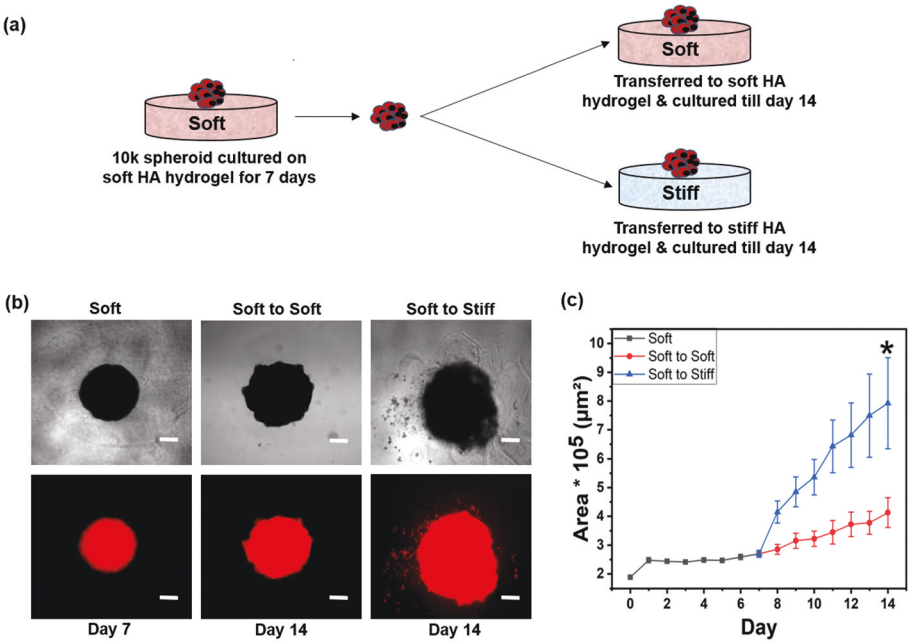

Fig. 4 Stiffness induced dormant phenotype observed on the soft HA hydrogel (0.4 kPa) for 10k cell spheroids was reversible. (a) Schematic depicting the transfer of 10k cell spheroids from the soft HA hydrogel to another soft or stiff HA hydrogel. (b) Day 7 bright field and fluorescent images of 10k cell spheroids cultured on the soft HA hydrogel and day 14 bright field and fluorescent images of 10k cell spheroids transferred from the soft HA hydrogel on day 7 to the soft or stiff HA hydrogel and cultured for an additional 7 days. Scale bar = 200 μm. (c) Area of 10k cell spheroids measured over a period of 14 days. $N \geq 6$ replicated per condition. *Indicates statistical significance ($p < 0.05$) compared to the 'soft to soft' condition for the area at day 14. Error bar represents standard error.

induced dormant phenotype was reversible. Specifically, we tested whether the transfer of a dormant spheroid to a stiff HA hydrogel environment would revoke dormancy. For this study, 10k cell spheroids were cultured on a soft HA hydrogel for a period of 7 days, following which, the spheroids were collected and transferred on to a freshly prepared soft or stiff HA hydrogel (Fig. 4a) and cultured for an additional 7 days. On the soft HA hydrogel, 10k cell spheroids exhibited a dormant phenotype for the initial 7 days and later when transferred to a new soft HA hydrogel (soft to soft) showed a similar phenotype until day 14. Upon transfer to a stiff HA hydrogel (soft to stiff), cell migration from the spheroid was observed (Fig. 4b), but surprisingly, the formation of micro-colonies was not observed during the culture period. Furthermore, the area of the cell spheroids at day 14 for the soft to stiff HA hydrogel conditions was significantly higher ($p < 0.05$) when compared to soft to soft HA hydrogel conditions indicating a dormant-to-proliferative switch (Fig. 4c).

These results were further supported by Ki67 staining. In the case of spheroids cultured on soft to stiff HA hydrogel for 14 days, % of Ki67 positive cells were 2 fold higher ($p < 0.05$) when compared to the soft to soft HA hydrogel. In particular, 19.2 ± 1.6% of the cells were Ki67 positive in the soft to stiff HA hydrogel compared to 9.2 ± 0.8% in the soft to soft HA hydrogel (Fig. 5). In addition, we also evaluated whether the dormant spheroids could attain a proliferative phenotype when they were transferred to 2D TCPS (*i.e.*, soft to adherent) culture conditions. Herein, 10k cell spheroids were transferred to 2D TCPS after culturing on the soft HA hydrogel for 7 days. Transfer of these dormant spheroids to 2D TCPS also triggered the phenotypic switch from dormant to proliferative phenotype, over the course of 7 additional days in culture. Specifically, the area of the cell spheroids cultured in soft to adherent was significantly higher ($p < 0.05$) when compared to soft to soft conditions. Additionally, the % of Ki67 positive cells under soft to adherent conditions (34 ± 3%) was ~3.5 times higher compared to soft to soft conditions (9.2 ± 0.8%) (Fig. S22†). Modulation of the culture environment resulted in cell migration from spheroids similar to the observations made by Grandhi *et al.*,[28] whereas the spheroids retained dormant phenotype when cultured in a similar microenvironment (*i.e.*, soft HA hydrogel) (Fig. 4, 5 and S22†). Taken together, these results indicated that the observed dormant phenotype was, indeed, reversible by modulating the culture environment.

Some limitations of this study that should be taken into consideration are as follows: (i) *In vivo*, CTC clusters may also contain immune cells that can impact the growth of CTC clusters[5,53] and future studies should examine the interactions between CTC clusters and immune cells. (ii) Herein, the top-seeded culture was employed (as opposed to encapsulation) to specifically evaluate the impact of matrix stiffness and cluster size and future studies could examine how the encapsulation of cell clusters impacts their phenotype. Overall, by utilizing a biomimetic HA hydrogel platform to recapitulate the brain microenvironment, we elucidated metastatic site specific cell cluster–ECM interactions (*i.e.*, ECM stiffness induced dor-

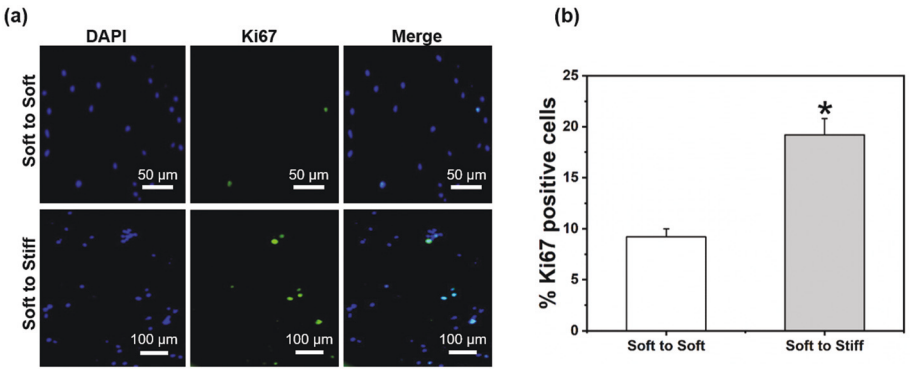

Fig. 5 Brain metastatic breast cancer cells in 10k cell spheroids expressed a higher percentage of Ki67 positivity at day 14 when transferred from the soft HA hydrogel (0.4 kPa) to stiff HA hydrogel (4.5 kPa) as compared to those transferred from soft to soft HA hydrogels. (a) Representative fluorescent images of Ki67 staining for MDA-MB-231Br cells in 10k cell spheroids cultured on the soft HA hydrogel for 7 days and transferred to the soft or stiff HA hydrogel and cultured for an additional 7 days, blue – DAPI (nucleus) and green – Ki67. (b) Quantification of Ki67 positive cells present in 10k cell spheroids on the soft or stiff HA hydrogel post transfer. $N = 4$ replicates per condition. *Indicates statistically significant difference ($p < 0.05$) compared to the 'soft to soft' condition. Error bar indicates standard error.

mancy, spheroid size dependent dormant *vs*. proliferative phenotypes, formation of micro-colonies, and reawakening of dormant cell spheroids) in a single *in vitro* platform.

4. Conclusions

Here, we successfully utilized biomimetic HA hydrogels with variable stiffnesses and six different sizes of cell spheroids to evaluate the impact of ECM stiffness and cluster size on the dormant *versus* proliferative phenotypes of brain metastatic breast cancer cell clusters. BCBM cell spheroids attained a dormant phenotype when cultured on soft HA hydrogels, whereas they exhibited a size-dependent switch between the dormant and proliferative phenotypes on stiff HA hydrogels (*i.e.*, proliferative phenotype ≥5000 cells < dormant phenotype). In addition, micro-colony formation was observed for 10k cell spheroid on stiff HA hydrogels. We also demonstrated that the stiffness induced dormancy was reversible. This system could provide a useful tool to investigate the signaling pathways involved in BCBM colonization by further incorporating various metastatic site specific cues (*e.g.*, cellular cues) along with the mechanical cues investigated in this work. In addition, this system could also be used for screening anti-metastatic drugs.

Conflicts of interest

The authors declare that there are no conflicts of interest.

Acknowledgements

This work was supported by the National Science Foundation (CBET 1749837 to S.R.) and The University of Alabama Graduate Council Fellowship (to R. K.).

References

1 D. Hanahan and R. A. Weinberg, *Cell*, 2000, **100**, 57–70.
2 G. P. Gupta and J. Massagué, *Cell*, 2006, **127**, 679–695.
3 A. A. Narkhede, L. A. Shevde and S. S. Rao, *Int. J. Cancer*, 2017, **141**, 1091–1109.
4 K. L. Harper, M. S. Sosa, D. Entenberg, H. Hosseini, J. F. Cheung, R. Nobre, A. Avivar-Valderas, C. Nagi, N. Girnius, R. J. Davis, E. F. Farias, J. Condeelis, C. A. Klein and J. A. Aguirre-Ghiso, *Nature*, 2016, **540**, 588–592.
5 M. Giuliano, A. Shaikh, H. C. Lo, G. Arpino, S. De Placido, X. H. Zhang, M. Cristofanilli, R. Schiff and M. V. Trivedi, *Cancer Res.*, 2018, **78**, 845–852.
6 N. Aceto, A. Bardia, D. T. Miyamoto, M. C. Donaldson, B. S. Wittner, J. A. Spencer, M. Yu, A. Pely, A. Engstrom, H. Zhu, B. W. Brannigan, R. Kapur, S. L. Stott, T. Shioda, S. Ramaswamy, D. T. Ting, C. P. Lin, M. Toner, D. A. Haber and S. Maheswaran, *Cell*, 2014, **158**, 1110–1122.
7 K. J. Cheung, V. Padmanaban, V. Silvestri, K. Schipper, J. D. Cohen, A. N. Fairchild, M. A. Gorin, J. E. Verdone, K. J. Pienta, J. S. Bader and A. J. Ewald, *Proc. Natl. Acad. Sci. U. S. A.*, 2016, **113**, E854–E863.
8 S. S. Rao, R. V. Kondapaneni and A. A. Narkhede, *J. Biol. Eng.*, 2019, **13**, 3–3.
9 S. Pradhan, J. L. Sperduto, C. J. Farino and J. H. Slater, *J. Biol. Eng.*, 2018, **12**, 37.
10 M. S. Sosa, P. Bragado and J. A. Aguirre-Ghiso, *Nat. Rev. Cancer*, 2014, **14**, 611–622.
11 S. Pradhan and J. H. Slater, *Biomaterials*, 2019, **215**, 119177.
12 A. A. Narkhede, J. H. Crenshaw, D. K. Crossman, L. A. Shevde and S. S. Rao, *Acta Biomater.*, 2020, **107**, 65–77.
13 N. Linde, G. Fluegen and J. A. Aguirre-Ghiso, *Adv. Cancer Res.*, 2016, **132**, 45–71.
14 C. M. Ghajar, *Nat. Rev. Cancer*, 2015, **15**, 238–247.
15 S.-Y. Park and J.-S. Nam, *Exp. Mol. Med.*, 2020, **52**, 569–581.
16 S. Paget, *Lancet*, 1889, **133**, 571–573.

17 D. Barkan, J. E. Green and A. F. Chambers, *Eur. J. Cancer*, 2010, **46**, 1181–1188.
18 J. Y. Lee and O. Chaudhuri, *ACS Biomater. Sci. Eng.*, 2018, **4**, 302–313.
19 D. Barkan, H. Kleinman, J. L. Simmons, H. Asmussen, A. K. Kamaraju, M. J. Hoenorhoff, Z.-Y. Liu, S. V. Costes, E. H. Cho, S. Lockett, C. Khanna, A. F. Chambers and J. E. Green, *Cancer Res.*, 2008, **68**, 6241–6250.
20 D. Barkan and J. E. Green, *J. Visualized Exp.*, 2011, 2914, DOI: 10.3791/2914.
21 L. H. El Touny, A. Vieira, A. Mendoza, C. Khanna, M. J. Hoenerhoff and J. E. Green, *J. Clin. Invest.*, 2014, **124**, 156–168.
22 H. R. Lee, F. Leslie and S. M. Azarin, *J. Biol. Eng.*, 2018, **12**, 12.
23 J. Y. Fang, S. J. Tan, Y. C. Wu, Z. Yang, B. X. Hoang and B. Han, *J. Transl. Med.*, 2016, **14**, 38.
24 Y. Liu, J. Lv, X. Liang, X. Yin, L. Zhang, D. Chen, X. Jin, R. Fiskesund, K. Tang, J. Ma, H. Zhang, W. Dong, S. Mo, T. Zhang, F. Cheng, Y. Zhou, J. Xie, N. Wang and B. Huang, *Cancer Res.*, 2018, **78**, 3926–3937.
25 Y. Kassim, E. Tawil, C. Buquet, D. Le Cerf and J. PierreVannier, *J. Clin. Exp. Oncol.*, 2017, **6**, 1000194.
26 J. Preciado, E. Reátegui, S. Azarin, E. Lou and A. Aksan, *Technology*, 2017, **5**, 1–10.
27 J. Schrader, T. T. Gordon-Walker, R. L. Aucott, M. van Deemter, A. Quaas, S. Walsh, D. Benten, S. J. Forbes, R. G. Wells and J. P. Iredale, *Hepatology*, 2011, **53**, 1192–1205.
28 T. S. Pavan Grandhi, T. Potta, R. Nitiyanandan, I. Deshpande and K. Rege, *Biomaterials*, 2017, **142**, 171–185.
29 R. Marlow, G. Honeth, S. Lombardi, M. Cariati, S. Hessey, A. Pipili, V. Mariotti, B. Buchupalli, K. Foster, D. Bonnet, A. Grigoriadis, P. Rameshwar, A. Purushotham, A. Tutt and G. Dontu, *Cancer Res.*, 2013, **73**, 6886–6899.
30 D. M. Sosnoski, R. J. Norgard, C. D. Grove, S. J. Foster and A. M. Mastro, *Clin. Exp. Metastasis*, 2015, **32**, 335–344.
31 S. E. Wheeler, A. M. Clark, D. P. Taylor, C. L. Young, V. C. Pillai, D. B. Stolz, R. Venkataramanan, D. Lauffenburger, L. Griffith and A. Wells, *Br. J. Cancer*, 2014, **111**, 2342–2350.
32 A. S. Khazali, A. M. Clark and A. Wells, *Br. J. Cancer*, 2018, **118**, 566–576.
33 L. Jadin, S. Pastorino, R. Symons, N. Nomura, P. Jiang, T. Juarez, M. Makale and S. Kesari, *Ann. Transl. Med.*, 2015, **3**, 80.
34 K. J. Wolf and S. Kumar, *ACS Biomater. Sci. Eng.*, 2019, **5**, 3753–3765.
35 B. Ananthanarayanan, Y. Kim and S. Kumar, *Biomaterials*, 2011, **32**, 7913–7923.
36 A. A. Narkhede, J. H. Crenshaw, R. M. Manning and S. S. Rao, *J. Biomed. Mater. Res., Part A*, 2018, **106**, 1832–1841.
37 A. Ivascu and M. Kubbies, *J. Biomol. Screening*, 2006, **11**, 922–932.
38 P. S. Nakod, Y. Kim and S. S. Rao, *Biotechnol. Bioeng.*, 2020, **117**, 511–522.
39 M. V. Monteiro, V. M. Gaspar, L. P. Ferreira and J. F. Mano, *Biomater. Sci.*, 2020, **8**, 1855–1864.
40 U. Grässer, M. Bubel, D. Sossong, M. Oberringer, T. Pohlemann and W. Metzger, *Ann. Anat.*, 2018, **216**, 1–8.
41 D. Barkan, L. H. El Touny, A. M. Michalowski, J. A. Smith, I. Chu, A. S. Davis, J. D. Webster, S. Hoover, R. M. Simpson, J. Gauldie and J. E. Green, *Cancer Res.*, 2010, **70**, 5706–5716.
42 S. S. Rao, J. DeJesus, A. R. Short, J. J. Otero, A. Sarkar and J. O. Winter, *ACS Appl. Mater. Interfaces*, 2013, **5**, 9276–9284.
43 Y. Jamin, J. K. R. Boult, J. Li, S. Popov, P. Garteiser, J. L. Ulloa, C. Cummings, G. Box, S. A. Eccles, C. Jones, J. C. Waterton, J. C. Bamber, R. Sinkus and S. P. Robinson, *Cancer Res.*, 2015, **75**, 1216–1224.
44 A. N. May, B. D. Crawford and A. M. Nedelcu, *Front. Oncol.*, 2018, **8**, 63.
45 M. G. Ondeck, A. Kumar, J. K. Placone, C. M. Plunkett, B. F. Matte, K. C. Wong, L. Fattet, J. Yang and A. J. Engler, *Proc. Natl. Acad. Sci. U. S. A.*, 2019, **116**, 3502–3507.
46 M. Sobecki, K. Mrouj, J. Colinge, F. Gerbe, P. Jay, L. Krasinska, V. Dulic and D. Fisher, *Cancer Res.*, 2017, **77**, 2722–2734.
47 T. Scholzen and J. Gerdes, *J. Cell. Physiol.*, 2000, **182**, 311–322.
48 A. Salic and T. J. Mitchison, *Proc. Natl. Acad. Sci. U. S. A.*, 2008, **105**, 2415.
49 B. D. Lehmann, J. A. Bauer, X. Chen, M. E. Sanders, A. B. Chakravarthy, Y. Shyr and J. A. Pietenpol, *J. Clin. Invest.*, 2011, **121**, 2750–2767.
50 M. Singh, S. Mukundan, M. Jaramillo, S. Oesterreich and S. Sant, *Cancer Res.*, 2016, **76**, 3732–3743.
51 M. Singh, H. Venkata Krishnan, S. Ranganathan, B. Kiesel, J. H. Beumer, S. Sreekumar and S. Sant, *ACS Biomater. Sci. Eng.*, 2018, **4**, 421–431.
52 L. A. Kunz-Schughart, J. P. Freyer, F. Hofstaedter and R. Ebner, *J. Biomol. Screening*, 2004, **9**, 273–285.
53 K. Leone, C. Poggiana and R. Zamarchi, *Diagnostics*, 2018, **8**, 59.

